ACS OMEGA

http://pubs.acs.org/journal/acsodf

Article

Heteroleptic Triple-Stranded Metallosupramolecules with Hydrophobic Inner Voids

Thanh Nhan Nguyen, Ngoc Minh Tran, In-Hyeok Park,* and Hyojong Yoo*

Cite This: *ACS Omega* 2022, 7, 13067−13074

Read Online

ACCESS | Metrics & More | Article Recommendations | Supporting Information

ABSTRACT: The systematic combination of well-defined coordination spheres and multiple types of ligands (heteroleptic) can lead to the generation of hierarchical metallosupramolecules with a high level of complexity and functionality. In particular, a specific multilevel coordination-driven assembly through the initiate generation of multinuclear clusters can form unique heteroleptic multiple-stranded supramolecular complexes. Herein, we report novel triple-stranded nickel-based supramolecules constructed from two different ditopic ligands ([1,1′:3′,1′′-terphenyl]-4,4′′-dicarboxylate (TP) and 2,6-pyridinedicarboxylate (PDA)) and a nickel precursor. The solid-state structures of the as-synthesized supramolecules revealed that three PDA ligands are employed to fabricate a tetranuclear ({Ni_4}) cluster, and two {Ni_4} clusters are assembled to form the final triple-stranded metallosupramolecules by three TP ligands. The bridging TP ligands also provide large inner voids with highly hydrophobic environments. Structural investigation of the generated complexes provided a deeper understanding of the aspects driving the formation of heteroleptic supramolecules, which is crucial for the design of multiple-strands with desired morphologies and functionalities.

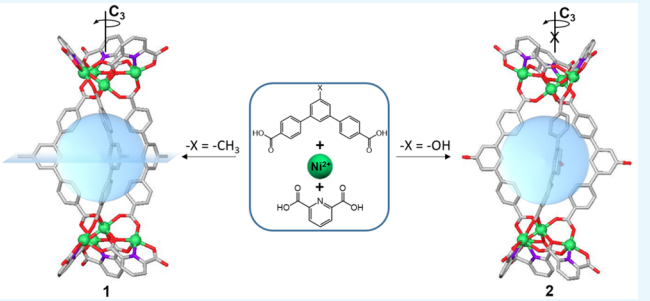

INTRODUCTION

Highly programmed metallosupramolecular assemblies have attracted intensive interest in mimicking the unique topologies of various natural structures.[1−4] To obtain a high level of intricacy and functionality, systematic combinations of metal ions with well-defined coordination and multiple types of ligands (heteroleptic) with proper geometric properties have been attempted,[5−8] and the resulting hierarchical structures have been applied in the construction of highly ordered systems,[9,10] energy conversion,[11−13] catalysis,[14] and enzyme mimics.[15] Each ligand in a heteroleptic supramolecule can have its own structural role in driving the assembly of primary metallic clusters or combining the clusters to generate secondary assemblies within a unique structural organization.[16] Efforts have been made to create heteroleptic metallosupramolecules. However, entropy often thwarts these efforts due to the high tendency to form uncontrolled statistical mixtures of homo- and heteroleptic supramolecules or narcissistically self-sorted mixtures.[17,18] Hence, the formation of a single, integratively self-sorted species needs to be driven by significant enthalpic benefit originated from the perfect combination of two types of ligand components in the assembly to overcome entropic penalty,[19−22] or the homoleptic structures are disfavored by repulsive steric or strain effects.[23]

Among various reported discrete supramolecular species up to now, helicates and mesocates are considered to be the simplest architectures.[24] The chirality of these two structural modes depends on the assembly of two chiral metal units. The combination of two units with the same configuration results in a chiral helicate. If two units of opposite configurations are combined, an achiral mesocate is formed.[25] The formation of helicate or mesocate greatly depends on the nature of the metal and ligands[26,27] and sometimes on additional information introduced by template[28] or reaction conditions.[29] For ligands, the stereoselectivity of the self-assembly can be influenced by ligand rigidity, ligand geometry, and the number of methylene units in the alkyl spacers.[30] Immense works have been done for the investigation of helicate and mesocate compounds, but the future will show the merit of studying this fascinating topic of metallosupramolecular chemistry.[25]

In our reported works, we have reported a range of supramolecules in which metal ions (Co^{2+}, Ni^{2+}, or Mn^{2+}) coordinated with 2,6-pyridinedicarboxylate (PDA) to form tetranuclear metal clusters (primary assembly), and two metal clusters are interlinked by three bridging ligands, that is, benzene-1,3-dicarboxylate (PTA) derivatives or 4,4′-carbonyldibenzoate (CDBA), to form triple-stranded helicates (TSH) with C_3 symmetry.[31−36] For supramolecules constructed from

Received: January 21, 2022
Accepted: March 25, 2022
Published: April 8, 2022

PTA derivative, three bridging ligands with a bending angle of 120° create an empty space within the supramolecule. Depending on the substituent/functional group attached to C5 of the PTA ligand, various higher-order assembly modes were obtained such as discrete, polymeric, and cage metallosupramolecules.[31−35] When moving from a one-benzene ring system (PTA) to a two-benzene ring system (CDBA), TSHs could also be obtained with C_3 symmetry.[36] The inner voids surrounded by three CDBA ligands are larger than those surrounded by three PTA derivative ligands. Meanwhile, the higher length and flexibility of CDBA initiate a higher potential for the generation of unprecedented higher-order assembly modes with high complexity, flexibility, and diversity. The maintenance of heteroleptic structures when changing metal ions, as well as extending the ligand length and flexibility, also suggests that the symmetry and helicity of triple-stranded metallosupramolecules are energetically favorable.[37]

On the basis of the results about metallosupramolecules we have obtained so far, we expect that the extension in bridging ligand length, together with the variation of the substituent/functional groups in the backbone, could create metallosupramolecules with unprecedented assembly modes. The lengthening of the bridging ligand is also expected to generate voids with large size, which is meaningful in host−guest interaction. Herein, 5′-methyl-[1,1′:3′,1′′-terphenyl]-4,4′′-dicarboxylate (CH_3-TP) and 5′-hydroxy-[1,1′:3′,1′′-terphenyl]-4,4′′-dicarboxylate (HO-TP) ligands were used to construct heteroleptic supramolecules. The V-shaped geometry with a bending angle of 120°, together with the significantly long distance between two terminal carboxyl groups and high flexibility of these ligands, generates discrete molecules with novel and unprecedented symmetries. In addition, the ligands can create an empty space within the supramolecule, which is promising for gas adsorption and catalysis.

EXPERIMENTAL SECTION

Materials and Methods. *Materials.* 5′-Methyl-[1,1′:3′,1′′-terphenyl]-4,4′′-dicarboxylic acid (CH_3-H_2TP) and 5′-hydroxy-[1,1′:3′,1′′-terphenyl]-4,4′′-dicarboxylic acid (HO-H_2TP) were prepared according to the method reported in the literature.[38−40] Other chemicals were purchased from commercial sources and used without further purification. Tetrakis(triphenylphosphine)palladium(0) ($Pd(PPh_3)_4$, 95%, Fluorochem), 3,5-dibromotoluene ($C_7H_6Br_2$, 98%, TCI), 3,5-dibromophenol ($C_6H_4Br_2O$, 98%, TCI), 4-carboxylphenylboronic acid ($C_7H_7BO_4$, 97%, Thermo Scientific), nickel(II) nitrate hexahydrate ($Ni(NO_3)_2{\cdot}6H_2O$, 97%, Sigma-Aldrich), nickel(II) acetate tetrahydrate ($Ni(OAc)_2{\cdot}4H_2O$, 98%, Sigma-Aldrich), 2,6-pyridinedicarboxylic acid (H_2PDA, $C_7H_5NO_4$, 99%, Sigma-Aldrich), N,N-dimethylformamide (DMF, 99.99%, Burdick and Jackson), hydrochloric acid (HCl, 35−37%, Samchun), nitric acid (68−70%, Samchun), potassium carbonate (K_2CO_3, 99.0%, TCI), methanol (Samchun, 99.5%), dichloromethane (CH_2Cl_2, 99.9%, Duksan), and acetone (99.96%, Burdick and Jackson) were used as received.

Syntheses. *Synthesis of CH_3-H_2TP (5′-Methyl-[1,1′:3′,1′′-terphenyl]-4,4′′-dicarboxylic acid) and HO-H_2TP (5′-Hydroxy-[1,1′:3′,1′′-terphenyl]-4,4′′-dicarboxylic acid).* The synthesis of CH_3-H_2TP ligand was according to a method proposed in the literature with a slight modification.[38−40] In a typical synthesis, 3,5-dibromotoluene (2.00 g, 8.00 mmol) and 4-carboxylphenylboronic acid (3.98 g, 24.0 mmol) were dissolved in potassium carbonate solution (16.0 g, in 93 mL H_2O) and 180 mL of dimethylformamide (DMF) in a 500 mL Schlenk flask. The resulting mixture was stirred vigorously and degassed for 30 min. After that, tetrakis(triphenylphosphine)-palladium(0) (1.27 g, 1.10 mmol) was added quickly to the flask, and the system was degassed for a further 10 min. The Schlenk flask was sealed and stirred at 100 °C for 3 days. The reaction mixture after cooling down to room temperature (RT) was poured into 100 mL of H_2O and washed with dichloromethane (5 × 100 mL). The water phase was separated and acidified with an aqueous HCl solution (v/v = 1:1). The product was collected by centrifugation at 4500 rpm for 3 min, washed with water four times, and finally washed with methanol. The resulting white solid was dried in an oven at 90 °C for 24 h to give CH_3-H_2TP ligand in 55.3% yield (based on the amount of 3,5-dibromotoluene used). The ^{1}H NMR spectrum of the CH_3-H_2TP ligand is shown in Figure S1.

HO-H_2TP ligand was synthesized using a similar protocol, with the exception that 3,5-dibromophenol was used instead of 3,5-dibromotoluene. The product yield was 58.6% based on the amount of 3,5-dibromophenol used. Figure S2 shows the ^{1}H NMR spectrum of the HO-H_2TP ligand.

*Synthesis of $[Ni_8(PDA)_6(CH_3\text{-}TP)_3(H_2O)_6]$ (**1**).* DMF solutions of $Ni(NO_3)_2{\cdot}6H_2O$ (1.2 mL, 0.05 M), H_2PDA (0.6 mL, 0.05 M), CH_3-H_2TP (0.3 mL, 0.05 M), and HNO_3 (0.1 mL, 0.05 M) were mixed in a 4 mL glass vial at RT. The vial was sealed, heated to 100 °C (heating rate; 2.67 °C/min), maintained for 24 h, and then cooled to 30 °C (cooling rate; −0.25 °C/min). After the cooling process, green hexagonal plate-shaped crystals of **1**, suitable for SC-XRD analysis, were successfully formed and sequentially washed with DMF (3 × 10 mL) and acetone (3 × 10 mL) and then dried in vacuo. The solid yield of **1** was 37.3% based on H_2PDA. Anal. Calcd. for $C_{105}H_{72}N_6O_{42}Ni_8$ (FW = 2559.36 g/mol): C: 49.27, H: 2.84, N: 3.28. Found: C: 49.85, H: 4.28, N: 5.58.

*Synthesis of $[Ni_8(PDA)_6(HO\text{-}TP)_3(DMF)_3(H_2O)_3]$ (**2**).* The synthesis of **2** was similar to that of **1**, except for the use of different precursors. Specifically, a mixture of $Ni(OAc)_2{\cdot}4H_2O$ (1.2 mL, 0.05 M), H_2PDA (0.6 mL, 0.05 M), HO-H_2TP (0.3 mL, 0.05 M), and HCl (0.1 mL, 1.00 M) was used. Compound **2** was obtained as green rod-shaped crystals with a solid yield of 40.5% based on H_2PDA. Anal. Calcd. for $C_{111}H_{81}N_9O_{45}Ni_8$ (FW = 2730.41g/mol): C: 48.78, H: 2.97, N: 4.61. Found: 45.33, H: 4.10, N: 7.01.

Instrumentation. The ^{1}H nuclear magnetic resonance (^{1}H NMR) spectra of the organic ligands were recorded on a Bruker AVANCE III-400 instrument (400 MHz) using dimethyl sulfoxide-d_6 (DMSO-d_6) as the NMR solvent. Thermogravimetric analysis (TGA) and differential scanning calorimetry (DSC) were performed from RT to 600 °C at a heating rate of 10 °C/min under a nitrogen atmosphere using a Q600 simultaneous DSC-DTA-TGA system from TA Instruments. Powder X-ray diffraction (PXRD) was performed using synchrotron radiation (wavelength 1.1 Å) in focused beam configuration in the 2θ range of 2−30° at 298 K. The simulated PXRD patterns were calculated from the single-crystal X-ray diffraction (SC-XRD) data using the Mercury 3.8 program. X-ray photoelectron spectroscopy (XPS) measurement was performed on an R3000 spectrometer (VG SCIENTA, United Kingdom) with monochromated Al Kα X-ray radiation as the X-ray source for excitation. Magnetic measurements of compounds were performed using a

https://doi.org/10.1021/acsomega.2c00447
ACS Omega 2022, 7, 13067−13074

Quantum Design MPMS3 magnetometer for temperatures 3 K ≤ T ≤ 300 K with a 1000 Oe applied field.

X-ray Crystallography. Diffraction data obtained from the light green crystals of (**1**) (0.117 × 0.094 × 0.084 mm^3) and (**2**) (0.105 × 0.058 × 0.027 mm^3) mounted on a MiTeGen MicroMount were collected at 223 K (for **1**) and 293 K (for **2**) on a Rayonix MX225HS detector with a silicon (111) double-crystal monochromator (DCM) equipped with a synchrotron radiation source (0.80000 and 0.70000 Å for **1** and **2**, respectively) at the 2D Supramolecular Crystallography Beamline (2D SMC), Pohang Accelerator Laboratory (PAL), Pohang, Republic of Korea. All of the calculations for the structure determination were carried out using the SHELXTL package (Ver. 2018/3).

RESULTS AND DISCUSSION

CH_3-H_2TP (5′-methyl-[1,1′:3′,1′′-terphenyl]-4,4′′-dicarboxylic acid) and HO-H_2TP (5′-hydroxy-[1,1′:3′,1′′-terphenyl]-4,4′′-dicarboxylic acid) were synthesized through a Suzuki coupling reaction according to the method reported in the literature with a slight modification.[38−40] Similar to H_2PTA (benzene-1,3-dicarboxylic acid) and H_2CDBA (4,4′-carbonyldibenzoic acid) used in the syntheses of the previously reported triple-stranded supramolecules,[31−36] both CH_3-H_2TP and HO-H_2TP are ditopic ligands with a bending angle of ∼120° (Scheme 1). The fundamental difference between substituted H_2TP ligands and H_2PTA or H_2CDBA lies in their length and flexibility, that is, the distance between the carbon atoms in the two carboxyl groups of H_2TP ligand is significantly longer than those of H_2PTA and H_2CDBA (Scheme 1). In addition, H_2TP ligands show a higher level of flexibility when compared to H_2PTA or H_2CDBA, which can be mainly attributed to the rotations around the two single C−C bonds connected to the central phenyl ring.

Scheme 1. Chemical Structures of Ligands That Have Been Used to Synthesize Heteroleptic Triple-Stranded Supramolecules: H_2PDA, H_2PTA Derivatives (X-H_2PTA, X = −H, −tbu, −OH, −Br, −I, −NH_2), H_2CDBA (Previous Works), and H_2TP Derivatives (X-H_2TP, X = −CH_3, −OH) (This Work)

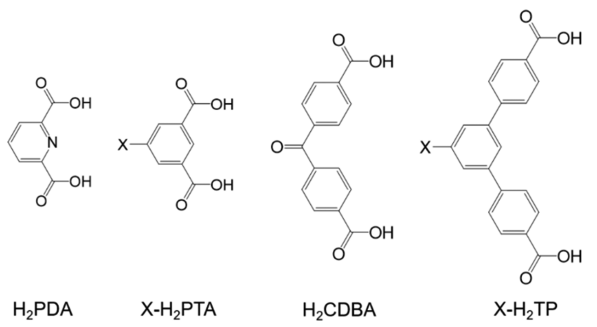

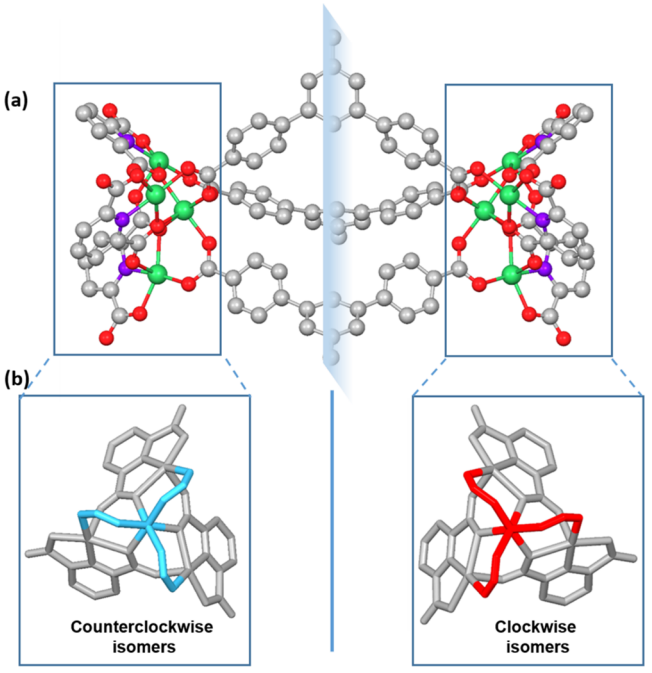

Figure 1. X-ray crystal structure of $[Ni_8(PDA)_6(CH_3\text{-}TP)_3(H_2O)_6]$ (**1**). (a) Side view of **1** with two $\{Ni_4\}$ clusters linked by three CH_3-TP ligands, together with a mirror plane of symmetry in **1** (green balls show cobalt, purple parts show nitrogen, and red parts show oxygen). All the coordinated and free solvent molecules, hydrogen atoms, and disorder components were omitted for clarity. (b) Presentation of two nickel clusters in form of clockwise and counterclockwise isomers.

Treatment of 4 equiv of $Ni(NO_3)_2{\cdot}6H_2O$ with 2 equiv of H_2PDA and 1 equiv of CH_3-H_2TP in DMF with HNO_3 at 100 °C led to the formation of $[Ni_8(PDA)_6(CH_3\text{-}TP)_3(H_2O)_6]$ (**1**), which was isolated as a green crystalline product (Figure S3a and Scheme 2). The structure of **1** in the solid state was analyzed using single-crystal X-ray crystallography (SC-XRD)

Scheme 2. Schematic Representation for the Formation of 1 and 2

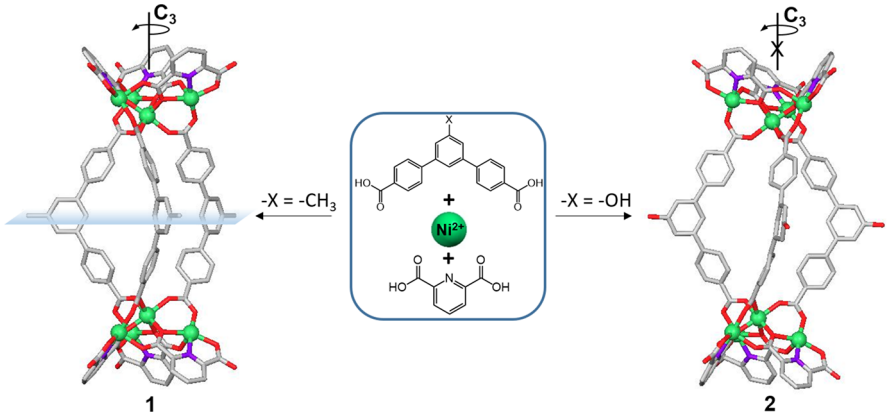

https://doi.org/10.1021/acsomega.2c00447
ACS Omega 2022, 7, 13067−13074

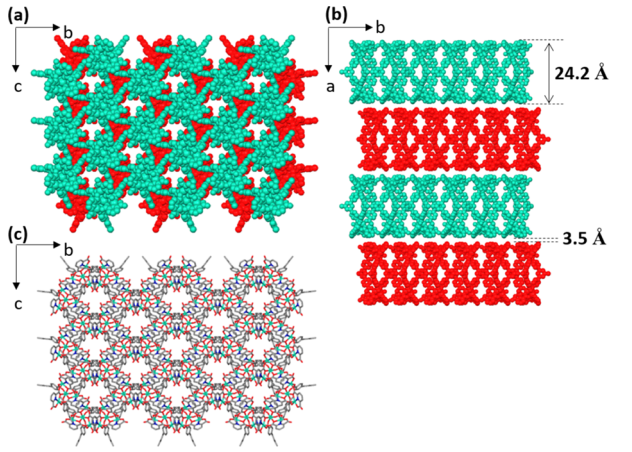

Figure 2. Packing structures of **1**. Space-filling representations of **1** from the views of the crystallographic (a) *a*-axis and (b) *c*-axis, showing the staggered assembly of adjacent packing layers of **1**. (c) Capped sticks representation of **1** illustrating its honeycomb packing structure.

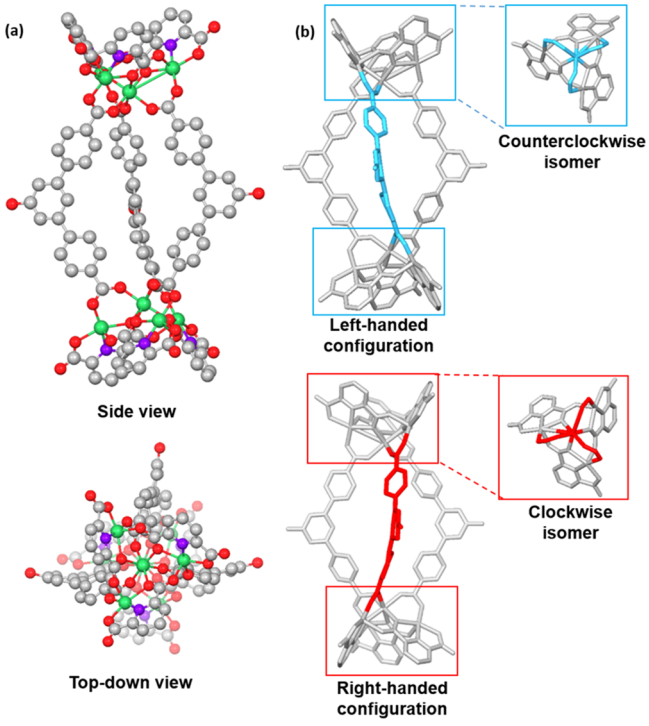

Figure 3. X-ray crystal structure of $[Ni_8(PDA)_6(HO\text{-}TP)_3(DMF)_3H_2O)_3]$ (**2**). (a) Side view and top-down view of **2**. (b) Representation of the left-handed and right-handed configurations of **2** with the respective constructing clusters.

(Figure 1a and Table S1), and the data were solved and refined as the orthorhombic group of *Ama*2. The solid-state structure revealed that **1** is composed of two tetranuclear nickel-based clusters {Ni_4}, bridged by three CH_3-TP ligands at nickel sites. Each cluster contains four nickel cations with a pseudo-octahedral geometry. The central nickel site is linked to three terminal nickels by three PDA ligands and linked to the other central nickel site by three CH_3-TP ligands. The terminal nickels are coordinated with two PDA ligands, one CH_3-TP ligand, and one water molecule (Figure S4). Note that the coordinated solvents in terminal nickels may not be the same in every experiment. The metal clusters possess chirality, either clockwise or counterclockwise, which is similar to the reported structures.[31−36] Each discrete supramolecule of **1** is constructed from two metal clusters with opposite chirality, resulting in a meso-helicate (Figure 1). The existence of one mirror plane of symmetry passing through the middle point of the three CH_3-TP ligands initiates C_{3h} symmetry of the meso-helicate. This is unique when compared to the reported triple-stranded supramolecules,[31−36] which show two metal clusters of the same chirality interconnected via three PTA derivative or CDBA bridging ligands, leading to the formation of either right-handed or left-handed helicate with C_3 symmetry. In terms of crystal packing, the discrete molecules of **1** are arranged regularly into layers. Every two adjacent layers are staggered and separated by a gap of 3.5 Å (Figure 2a,b). Every alternating layer is eclipsed, resulting in the formation of honeycomb-shaped one-dimensional channels (Figure 2b,c).

The phase purity of the as-synthesized **1** was determined using powder X-ray diffraction (PXRD) (Figure S5). There are considerable similarities between the observed and the expected PXRD patterns. Thermogravimetric analysis (TGA) and differential scanning calorimetry (DSC) of **1** were shown in Figure S6. The first weight loss of 6.1% up to 168 °C is assigned to the loss of coordinated solvent within **1** and the next weight loss of 56.1% up to 600 °C corresponds to the decomposition of organic ligands.[31] The endothermic peaks and weight loss observed from DSC and TGA curves at 350−420 °C indicate that the thermal decomposition of **1** occurred rapidly at this temperature range. XPS full spectrum confirmed the presence of Ni, O, C, and N in **1** (Figure S7a). The deconvolution of high-resolution O 1s XPS spectrum indicates the present C−O (530.8 eV), C−O−Ni (532.0 eV), and C═O (533.0 eV),[41] while the deconvolution of high-resolution N 1s XPS spectrum suggests the existence of N (pyridine) (398.7 eV) and N (amide) (399.9 eV) in **1** (Figure S7b,c).[42,43] The oxidation state of nickel ions was determined to be +2 by the presence of two strong peaks at 855.98 and 873.11 eV standing for Ni $2p_{3/2}$ and Ni $2p_{1/2}$, respectively (Figure S7d).[35,36] The bond valence sum calculation also revealed that nickel ions in these clusters have a +2 oxidation state (Table S2).[44,45] The measurement of temperature-dependent magnetization (emu/g) of **1** was conducted using a Quantum Design MPMS3 magnetometer for temperatures 3 K ≤ T ≤ 300 K with 1000 Oe applied fields (Figure S8a). By applying the Curie−Weiss law, the corresponding fitting ($1/\chi$ vs T) (Figure S8b) yielded a Weiss constant θ = −7.78 K, suggesting the week antiferromagnetic interaction between nickel ions,[46] and Curie−Weiss constant C = 0.00383 emu K g^{-1}. The measured $\chi_M T$ at 300 K was 1.20 (emu K mol^{-1}) (Figure S8c), and the corresponding μ_{eff} was calculated to be 3.10 μ_B This value falls within an acceptable range of experimentally observed high-spin octahedral Ni (II) ions.[47]

The inner empty space of **1**, as illustrated in Figure S9, is noticeable. The size of this "inner cage" is significantly larger than the similar empty spaces of the previously reported triple-stranded supramolecules prepared using PTA or CDBA ligands.[31−36] The larger size of the inner space of **1** possibly allows the inclusion of external molecules through further ligand modification. In general, the hydrophobicity of a cage can be proved by the inclusion of hydrophobic molecules from the water phase.[48] It was also commented that the central cavity of a cage may be hydrophobic owing to its surrounding aryl rings.[48−50] Therefore, the empty space inside **1**, which is

https://doi.org/10.1021/acsomega.2c00447
ACS Omega 2022, 7, 13067−13074

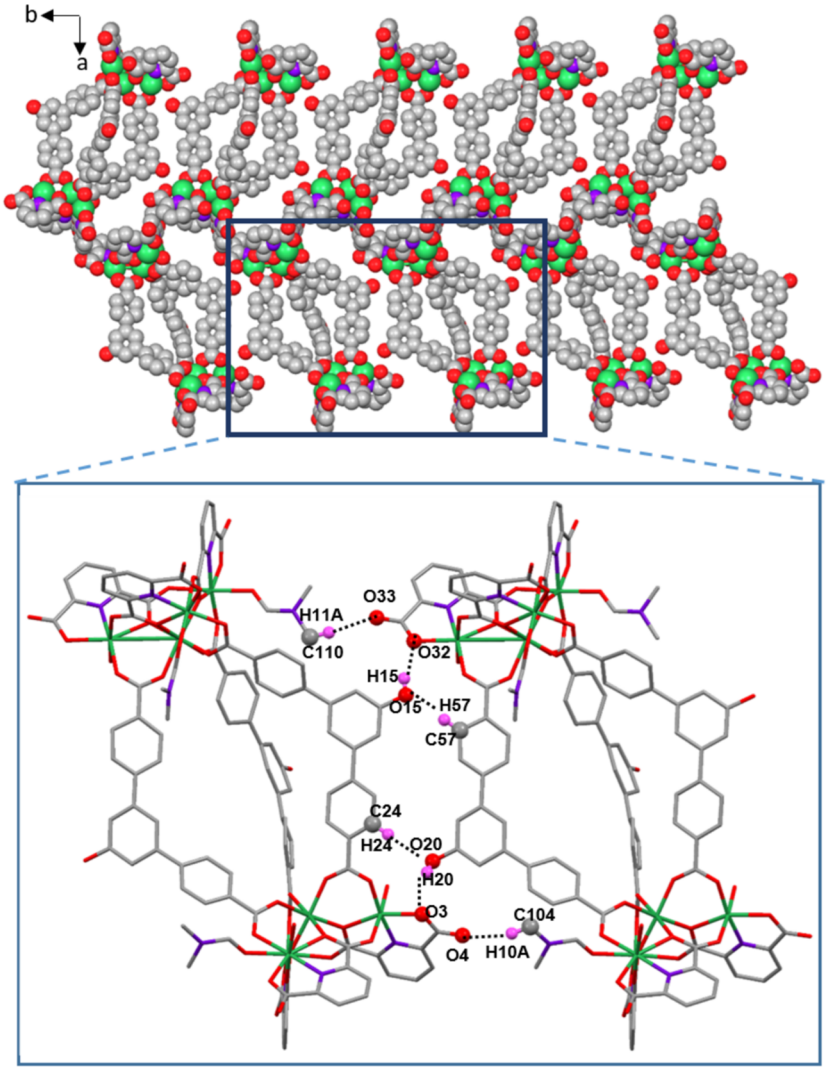

Figure 4. Higher-order assembly of **2** with the representation of the numerous intermolecular interactions formed between adjacent discrete supramolecules.

surrounded by aryl rings, can be regarded as hydrophobic. Moreover, using SQUEEZE,[51] we could confirm that solvent molecules were excluded from the void. Hence, we speculate that the inner voids are highly hydrophobic. The numerous C−H bonds in the aromatic rings are oriented toward the inner space, providing the possibility for host−guest interactions including hydrophobic and CH···π interactions.[52,53] Thus, these inner empty spaces may exhibit selectivity toward neutral and hydrophobic guests because of the hydrophobic effect.[48,54] In addition, the hydrophobic inner voids can be further applied as a reactor due to their ability to provide a suitable environment for hosting chemical reactions, as well as stabilizing reactive hydrophobic intermediates.[48,55]

The effects of bridging ligand modification on the self-assembly of heteroleptic supramolecules were also investigated with HO-TP ligand. Four equiv of $Ni(OAc)_2{\cdot}4H_2O$, 2 equiv of H_2PDA, and 1 equiv of HO-H_2TP were treated in DMF with HNO_3 at 100 °C, forming $[Ni_8(PDA)_6(HO\text{-}TP)_3(DMF)_3(H_2O)_3]$ (**2**) (Scheme 2 and Figure S3b). The solid-state structure of **2** shows multinuclear clusters of either clockwise or counterclockwise isomer (Figures 3 and S10). Different from **1**, two $\{Ni_4\}$ clusters are connected by three bridging ligands with unequal twisting, leading to the symmetry breaking in the structure (Figure 3a). The combination of two nickel clusters of the same chirality in a single supramolecule results in a helicate of either left-handed or right-handed configuration (Figure 3b). PXRD spectra of **2** show a good match between the experimental and the simulated patterns (Figure S11). The thermal property of **2** was shown in Figure S12. The first weight loss of 6.1% up to 168 °C is assigned to the removal of coordinated solvent, and the next weight loss of 56.1% up to 450 °C corresponds to the decomposition of organic ligands.[31] The fast decomposition at the temperature range of 360−430 °C was indicated not only by the dramatic weight loss but also the thermal event observed on the DSC curve at this condition. XPS full spectra confirmed the presence of Ni, O, C, and N in **2** (Figure S13a). The deconvolution of high-resolution O 1s XPS spectrum indicates the presence of O in the form of C−O, C−O−Ni, and C═O,[41] while the deconvolution of the high-resolution N 1s XPS spectrum suggests the existence of pyridine nitrogen and amide nitrogen in **2** (Figure S13b,c).[42,43] The +2 oxidation state of the nickel ions was confirmed with two strong peaks at 856.69 and 873.94 eV corresponding to Ni $2p_{3/2}$ and Ni $2p_{1/2}$, respectively (Figure S13d).[35,36] Using the bond valence sum theory, the oxidation state of the nickel ions in the clusters was

https://doi.org/10.1021/acsomega.2c00447
ACS Omega 2022, 7, 13067−13074

determined to be +2 (Table S2).[44,45] The temperature-dependent magnetization (emu/g) of **2** is illustrated in Figure S14a. The Curie–Weiss fitting ($1/\chi$ vs T) (Figure S14b) yielded a Weiss constant θ = −8.06 K, indicating the week antiferromagnetic interaction between nickel ions[46] and Curie–Weiss constant C = 0.00386 emu K g^{-1}. The value of $\chi_M T$ at 300 K was 1.31 (emu K mol^{-1}) (Figure S14c), and the corresponding μ_{eff} was 3.23 μ_B, which falls within an acceptable range of experimentally observed high-spin octahedral Ni (II) ions.[47]

The crystal packing of **2** revealed that the supramolecules are stacked by intermolecular interactions composed of numerous O–H···O and C–H···O hydrogen bonds (Figure 4). The estimated hydrogen bond lengths and bond angles of these interactions were summarized in Table S3. Notably, the O···O distances in O20–H20···O3 and O15–H15···O32 hydrogen bonds are 2.658 and 2.648 Å, significantly less than the sum of van der Waal radii of two oxygen atoms (3.04 Å), indicating that these hydrogen bonds are strong.[56−59] Considering the C104–H10A···O4 and C24–H24···O20 hydrogen bonds, although the C···O distances are 3.327 and 3.440 Å, which are longer than the sum of van der Waals radii of carbon and oxygen (3.22 Å), the H···O distances are 2.399 and 2.586 Å, less than the Van der Waals radii sum of hydrogen and oxygen (2.62 Å).[57] In addition, their bond angles are 165.3 and 128.6°, which are in the range of a common hydrogen bond (110–180°).[60] These data indicate that the formation of two C–H···O bonds is relatively effective. Although the H···O distances in C57–H57···O15 and C110–H11A···O33 are 2.694 and 2.703 Å, respectively, which are higher than the sum of Van der Walls radii of hydrogen and oxygen, it does not mean that no interaction exists. Instead, it suggests that these two hydrogen bonds can contribute to the stabilization energy but to a lesser extent than the four aforementioned hydrogen bonds. We assume that the stabilization energy from the various O–H···O and C–H···O hydrogen bonds compensated for the loss of entropy and the increase in enthalpy owing to the symmetry breaking of **2**.

CONCLUSION

In conclusion, two distinctive triple-stranded metallosupramolecules with unprecedented symmetries were successfully synthesized by extending the bridging ligand from a one- to a three-benzene-ring system with a longer length, higher flexibility, and variation in functional groups. While the assembly of tetranuclear clusters is similar in **1** and **2**, the different modes of combining two nickel clusters into a discrete supramolecule and the dissimilarity in linker geometries lead to the fabrication of meso-helicate **1** with very high symmetry (C_{3h}) and helicate **2** with no symmetry element. The combination of nickel clusters and TP derivative ligands generates a large empty space that can play the vital roles of a reactor or host–guest interaction.

ASSOCIATED CONTENT

Supporting Information

The Supporting Information is available free of charge at https://pubs.acs.org/doi/10.1021/acsomega.2c00447.

Details of crystallographic data, additional figures of metallosupramolecules, characterization data of ligands (^{1}H NMR), characterization data of supramolecules (XPS, PXRD, TGA-DSC, and magnetic property), calculation of sizes of inner voids of supramolecules (PDF)

Collection of two molecules (CIF)

Accession Codes

CCDC 2132311 and 2132320 contain the supplementary crystallographic data which can be obtained free of charge via www.ccdc.cam.ac.uk/data_request/cif, or by emailing data_request@ccdc.cam.ac.uk, or by contacting The Cambridge Crystallographic Data Centre, 12 Union Road, Cambridge CB2 1EZ, UK; fax: + 44 1223 336033.

AUTHOR INFORMATION

Corresponding Authors

In-Hyeok Park − *Graduate School of Analytical Science and Technology (GRAST), Chungnam National University, Daejeon 34134, Republic of Korea;* orcid.org/0000-0003-1371-6641; Email: ipark@cnu.ac.kr

Hyojong Yoo − *Department of Materials Science and Chemical Engineering, Hanyang University, Ansan, Gyeonggi-do 15588, Republic of Korea;* orcid.org/0000-0002-4932-3885; Email: hjhaha73@hanyang.ac.kr

Authors

Thanh Nhan Nguyen − *Department of Materials Science and Chemical Engineering, Hanyang University, Ansan, Gyeonggi-do 15588, Republic of Korea;* orcid.org/0000-0001-6338-3473

Ngoc Minh Tran − *Department of Materials Science and Chemical Engineering, Hanyang University, Ansan, Gyeonggi-do 15588, Republic of Korea;* orcid.org/0000-0003-2116-6707

Complete contact information is available at: https://pubs.acs.org/10.1021/acsomega.2c00447

Notes

The authors declare no competing financial interest.

ACKNOWLEDGMENTS

This research was supported by the National Research Foundation of Korea (NRF) grant funded by the Korea government (MSIP) (NRF-2020R1A2C1004006 and NRF-2021R1C1C1006765). Experiments at PLS-II were supported in part by MSIP and POSTECH (2021-first-2D-019, 2021-second-2D-023, and 2021-third-2D-032). Magnetic measurements were performed using facilities at IBS Center for Correlated Electron Systems, Seoul National University.

ABBREVIATIONS

CH_3-TP, 5′-methyl-[1,1′:3′,1′′-terphenyl]-4,4′′-dicarboxylate; HO-TP, 5′-hydroxy-[1,1′:3′,1′′-terphenyl]-4,4′′-dicarboxylate; H_2TP, [1,1′:3′,1′′-terphenyl]-4,4′′-dicarboxylic acid; TP, [1,1′:3′,1′′-terphenyl]-4,4′′-dicarboxylate; CDBA, 4,4′-carbonyldibenzoate

REFERENCES

(1) Neogi, S.; Lorenz, Y.; Engeser, M.; Samanta, D.; Schmittel, M. Heteroleptic Metallosupramolecular Racks, Rectangles, and Trigonal Prisms: Stoichiometry-Controlled Reversible Interconversion. *Inorg. Chem.* **2013**, *52*, 6975−6984.

(2) Wang, Y. S.; Feng, T.; Wang, Y. Y.; Hahn, F. E.; Han, Y. F. Homo- and Heteroligand Poly-NHC Metal Assemblies: Synthesis by Narcissistic and Social Self-Sorting. *Angew. Chem., Int. Ed.* **2018**, *57*, 15767−15771.

(3) De, S.; Mahata, K.; Schmittel, M. Metal-Coordination-Driven Dynamic Heteroleptic Architectures. *Chem. Soc. Rev.* **2010**, *39*, 1555−1575.
(4) Tessarolo, J.; Lee, H.; Sakuda, E.; Umakoshi, K.; Clever, G. H. Integrative Assembly of Heteroleptic Tetrahedra Controlled by Backbone Steric Bulk. *J. Am. Chem. Soc.* **2021**, *143*, 6339−6344.
(5) Wang, S.; Cheng, K.; Fu, J.; Cheng, Y.; Chan, Y. Conformational Regulation of Multivalent Terpyridine Ligands for Self-Assembly of Heteroleptic Metallo-Supramolecules. *J. Am. Chem. Soc.* **2020**, *142*, 16661−16667.
(6) He, L.; Wang, S.-C.; Lin, L.-T.; Cai, J.-Y.; Li, L.; Tu, T.-H.; Chan, Y.-T. Multicomponent Metallo-Supramolecular Nanocapsules Assembled from Calix[4]Resorcinarene-Based Terpyridine Ligands. *J. Am. Chem. Soc.* **2020**, *142*, 7134−7144.
(7) Palma, C. A.; Cecchini, M.; Samorí, P. Predicting Self-Assembly: From Empirism to Determinism. *Chem. Soc. Rev.* **2012**, *41*, 3713−3730.
(8) Holliday, B. J.; Mirkin, C. A. Strategies for the Construction of Supramolecular Compounds through Coordination Chemistry. *Angew. Chem., Int. Ed.* **2001**, *40*, 2022−2043.
(9) Pullen, S.; Clever, G. H. Mixed-Ligand Metal-Organic Frameworks and Heteroleptic Coordination Cages as Multifunctional Scaffolds - A Comparison. *Acc. Chem. Res.* **2018**, *51*, 3052−3064.
(10) Ahmadi, M.; Seiffert, S. Direct Evidence of Heteroleptic Complexation in the Macroscopic Dynamics of Metallo-Supramolecular Polymer Networks. *Macromolecules* **2021**, *54*, 7113−7124.
(11) Lifschitz, A. M.; Young, R. M.; Mendez-Arroyo, J.; Stern, C. L.; McGuirk, C. M.; Wasielewski, M. R.; Mirkin, C. A. An Allosteric Photoredox Catalyst Inspired by Photosynthetic Machinery. *Nat. Commun.* **2015**, *6*, 6541.
(12) Schmittel, M.; Kishore, R. S. K.; Bats, J. W. Synthesis of Supramolecular Fullerene-Porphyrin-Cu(Phen) 2-Ferrocene Architectures. A Heteroleptic Approach towards Tetrads. *Org. Biomol.-Chem.* **2007**, *5*, 78−86.
(13) Sozmen, F.; Oksal, B. S.; Bozdemir, O. A.; Buyukcakir, O.; Akkaya, E. U. Heteroleptic Metallosupramolecular Complexes of Bodipy Dyes as Energy Transfer Cassettes. *Org. Lett.* **2012**, *14*, 5286−5289.
(14) Brown, C. J.; Toste, F. D.; Bergman, R. G.; Raymond, K. N. Supramolecular Catalysis in Metal-Ligand Cluster Hosts. *Chem. Rev.* **2015**, *115*, 3012−3035.
(15) Yoon, H. J.; Kuwabara, J.; Kim, J. H.; Mirkin, C. A. Allosteric Supramolecular Triple-Layer Catalysts. *Science* **2010**, *330*, 66−69.
(16) Jansze, S. M.; Severin, K. Clathrochelate Metalloligands in Supramolecular Chemistry and Materials Science. *Acc. Chem. Res.* **2018**, *51*, 2139−2147.
(17) Zhu, R.; Bloch, W. M.; Holstein, J. J.; Mandal, S.; Schäfer, L. V.; Clever, G. H. Donor-Site-Directed Rational Assembly of Heteroleptic Cis-$[Pd_2L_2L'_2]$ Coordination Cages from Picolyl Ligands. *Chem.-Eur. J.* **2018**, *24*, 12976−12982.
(18) Bloch, W. M.; Abe, Y.; Holstein, J. J.; Wandtke, C. M.; Dittrich, B.; Clever, G. H. Geometric Complementarity in Assembly and Guest Recognition of a Bent Heteroleptic Cis-$[Pd_2LA_2LB_2]$ Coordination Cage. *J. Am. Chem. Soc.* **2016**, *138*, 13750−13755.
(19) Saha, S.; Regeni, I.; Clever, G. H. Structure Relationships between Bis-Monodentate Ligands and Coordination Driven Self-Assemblies. *Coord. Chem. Rev.* **2018**, *374*, 1−14.
(20) Wu, K.; Zhang, B.; Drechsler, C.; Holstein, J. J.; Clever, G. H. Backbone-Bridging Promotes Diversity in Heteroleptic Cages. *Angew. Chem., Int. Ed.* **2021**, *60*, 6403−6407.
(21) Bloch, W. M.; Clever, G. H. Integrative Self-Sorting of Coordination Cages Based on "naked" Metal Ions. *Chem. Commun.* **2017**, *53*, 8506−8516.
(22) Bardhan, D.; Chand, D. K. Palladium(II)-Based Self-Assembled Heteroleptic Coordination Architectures: A Growing Family. *Chem.-Eur. J.* **2019**, *25*, 12241−12269.
(23) Pullen, S.; Tessarolo, J.; Clever, G. H. Increasing Structural and Functional Complexity in Self-Assembled Coordination Cages. *Chem. Sci.* **2021**, *12*, 7269−7293.
(24) Romero, M. J.; Carballido, R.; Rodríguez-silva, L.; Maneiro, M.; Zaragoza, G.; González-noya, A. M.; Pedrido, R. An Unusual Assembled Pb(II) Meso-Helicate That Shows the Inert Pair Effect. *Dalton Trans.* **2016**, *45*, 16162−16165.
(25) Albrecht, M. Let's Twist Again" - Double-Stranded, Triple-Stranded, and Circular Helicates. *Chem. Rev.* **2001**, *101*, 3457−3497.
(26) Chinnaraja, E.; Arunachalam, R.; Suresh, E.; Sen, S. K.; Natarajan, R.; Subramanian, P. S. Binuclear Double-Stranded Helicates and Their Catalytic Applications in Desymmetrization of Mesodiols. *Inorg. Chem.* **2019**, *58*, 4465−4479.
(27) Romero, M. J.; Martinez-Calvo, M.; Maneiro, M.; Zaragoza, G.; Pedrido, R.; Gonzalez-Noya, A. M. Selective Metal-Assisted Assembly of Mesocates or Helicates with Tristhiosemicarbazone Ligands. *Inorg. Chem.* **2019**, *58*, 881−889.
(28) Chen, X.; Mevissen, C.; Huda, S.; Göb, C.; Oppel, I. M.; Albrecht, M. Cation-Controlled Formation and Interconversion of the *fac/fac* and *mer/mer* Stereoisomers of a Triple-Stranded Helicate. *Angew. Chem., Int. Ed.* **2019**, *58*, 12879−12882.
(29) Soumya, K. R.; Arumugam, R.; Shankar, B.; Sathiyendiran, M. Sulfate Donor Based Dinuclear Heteroleptic Triple-Stranded Helicates from Sulfite and Ditopic Nitrogen Donor Ligands and Their Transformation to Dinuclear Homoleptic Double-Stranded Mesocates. *Inorg. Chem.* **2018**, *57*, 10718−10725.
(30) Albrecht, M. How Do They Know ? Influencing the Relative Stereochemistry of the Complex Units of Dinuclear Triple-Stranded Helicate-Type Complexes. *Chem.-Eur. J.* **2000**, *6*, 3485−3489.
(31) Yoo, H.; Lee, J.; Kang, P.; Choi, M. G. Synthesis of Cobalt Cluster-Based Supramolecular Triple-Stranded Helicates. *Dalton Trans.* **2015**, *44*, 14213−14216.
(32) Mai, H. D.; Kang, P.; Kim, J. K.; Yoo, H. A Cobalt Supramolecular Triple-Stranded Helicate-Based Discrete Molecular Cage. *Sci. Rep.* **2017**, *7*, 43448.
(33) Mai, H. D.; Lee, I.; Yoo, H. Controllable Synthesis of a Highly Ordered Polymeric Structure Assembled from Cobalt-Cluster-Based Racemic Supramolecules. *Chem.-Asian J.* **2018**, *13*, 1915−1919.
(34) Kang, P.; Mai, H. D.; Yoo, H. Cage-like Crystal Packing through Metallocavitands within a Cobalt Cluster-Based Supramolecular Assembly. *Dalton Trans.* **2018**, *47*, 6660−6665.
(35) Thi Le, V. C.; Mai, H. D.; Kang, P.; Yoo, H. Metal-Ion Tuning in Triple-Stranded Helicate-Based Metallosupramolecules. *Chem.-Eur. J.* **2019**, *25*, 2472−2476.
(36) Kang, P.; Yoo, H. Coordinative Helix-Helix Association of Heteroleptic Metallosupramolecular Helicates. *Inorg. Chem. Front.* **2020**, *7*, 905−910.
(37) Tran, N. M.; Yoo, H. Recent Advances in Heteroleptic Multiple-Stranded Metallosupramolecules. *Dalton Trans.* **2020**, *49*, 11819−11827.
(38) Kitagawa, S.; Higuchi, M.; Kajiwara, T.; Higashimura, H.; Mochizuki, M.; Nagashima, K.; Kiyonaga, T. *Manufacture of Hydrocarbons by Cracking of C_4 or Higher Hydrocarbons with Porous Metal Complex Catalysts, Activation of Catalysts, and Measurement of Acid Strength of Catalysts*. Patent JP2014043435, 2014.
(39) Chen, Z.; Weselinski, Łu. J.; Adil, K.; Belmabkhout, Y.; Shkurenko, A.; Jiang, H.; Bhatt, P. M.; Guillerm, V.; Dauzon, E.; Xue, D.-X.; O'Keeffe, M.; Eddaoudi, M. Applying the Power of Reticular Chemistry to Finding the Missing Alb-MOF Platform Based on the (6,12)-Coordinated Edge-Transitive Net. *J. Am. Chem. Soc.* **2017**, *139*, 3265−3274.
(40) McHugh, L. N.; Cordes, D. B.; Wheatley, P. S.; Slawin, A. M. Z.; Morris, R. E. Synthetic and Crystallographic Investigation of the Layered Coordination Framework Copper-1,3-Bis(4-Carboxyphenyl)-5-Ethoxybenzene. *Cryst. Growth Des.* **2020**, *20*, 39−42.
(41) Yu, H. C.; Hao, X. P.; Zhang, C. W.; Zheng, S. Y.; Du, M.; Liang, S.; Wu, Z. L.; Zheng, Q. Engineering Tough Metallosupramolecular Hydrogel Films with Kirigami Structures for Compliant Soft Electronics. *Small* **2021**, *17*, 2103836.
(42) Jansen, R. J. J.; van Bekkum, H. XPS of Nitrogen-Containing Functional Groups on Activated Carbon. *Carbon* **1995**, *33*, 1021−1027.

https://doi.org/10.1021/acsomega.2c00447
ACS Omega 2022, 7, 13067−13074

(43) Lázaro Martínez, J. M.; Rodríguez-Castellón, E.; Sánchez, R. M. T.; Denaday, L. R.; Buldain, G. Y.; Campo Dall'Orto, V. XPS Studies on the Cu(I,II)-Polyampholyte Heterogeneous Catalyst: An Insight into Its Structure and Mechanism. *J. Mol. Catal. A Chem.* **2011**, *339*, 43−51.
(44) Brown, I. D. *Bond valence parameters*; IUCr, 2021. https://www.iucr.org/resources/data/datasets/bond-valence-parameters (accessed 10-13-2021).
(45) Brown, I. D. *The Chemical Bond in Inorganic Chemistry: The Bond Valence Model*; Oxford University Press: New York, 2002.
(46) Hatscher, S.; Schilder, H.; Lueken, H.; Urland, W. Practical Guide to Measurement and Interpretation of Magnetic Properties: IUPAC Technical Report. *Pure Appl. Chem.* **2005**, *77* (2), 497−509.
(47) Earnshaw, A. *Introduction to Magneto Chemistry*, 1st ed.; Academic Press: London, 1968.
(48) Yadav, S.; Kannan, P.; Qiu, G. Cavity-Based Applications of Metallo-Supramolecular Coordination Cages (MSCCs). *Org. Chem. Front.* **2020**, *7*, 2842−2872.
(49) Kusukawa, T.; Fujita, M. Encapsulation of Large, Neutral Molecules in a Self-Assembled Nanocage Incorporating Six Palladium(II) Ions. *Angew. Chem., Int. Ed* **1998**, *37*, 3142−3144.
(50) Yadav, A.; Sarkar, M.; Subrahmanyam, S.; Chaudhary, A.; Hey-Hawkins, E.; Boomishankar, R. Anilate Tethered Neutral Tetrahedral Pd(II) Cages Exhibiting Selective Encapsulation of Xylenes and Mesitylene. *Chem.-Eur. J.* **2020**, *26*, 4209−4213.
(51) Spek, A. L. PLATON SQUEEZE: a tool for the calculation of the disordered solvent contribution to the calculated structure factors. *Acta Crystallogr., Sect. C: Struct. Chem.* **2015**, *71*, 9−18.
(52) Jiao, J.; Li, Z.; Qiao, Z.; Li, X.; Liu, Y.; Dong, J.; Jiang, J.; Cui, Y. Design and Self-Assembly of Hexahedral Coordination Cages for Cascade Reactions. *Nat. Commun.* **2018**, *9*, 4423.
(53) Trembleau, L.; Rebek, J. Helical Conformation of Alkanes in a Hydrophobic Cavitand. *Science* **2003**, *301*, 1219−1220.
(54) Biros, S. M.; Bergman, R. G.; Raymond, K. N. The Hydrophobic Effect Drives the Recognition of Hydrocarbons by an Anionic Metal-Ligand Cluster. *J. Am. Chem. Soc.* **2007**, *129*, 12094−12095.
(55) Ahmad, N.; Chughtai, A. H.; Younus, H. A.; Verpoort, F. Discrete Metal-Carboxylate Self-Assembled Cages: Design, Synthesis and Applications. *Coord. Chem. Rev.* **2014**, *280*, 1−27.
(56) Arunan, E.; Desiraju, G. R.; Klein, R. A.; Sadlej, J.; Scheiner, S.; Alkorta, I.; Clary, D. C.; Crabtree, R. H.; Dannenberg, J. J.; Hobza, P.; Kjaergaard, H. G.; Legon, A. C.; Mennucci, B.; Nesbitt, D. J. Definition of the Hydrogen Bond (IUPAC Recommendations 2011). *Pure Appl. Chem.* **2011**, *83*, 1637−1641.
(57) Mantina, M.; Chamberlin, A. C.; Valero, R.; Cramer, C. J.; Truhlar, D. G. Consistent van Der Waals Radii for the Whole Main Group. *J. Phys. Chem. A* **2009**, *113*, 5806−5812.
(58) Corpinot, M. K.; Bučar, D. K. A Practical Guide to the Design of Molecular Crystals. *Cryst. Growth Des.* **2019**, *19*, 1426−1453.
(59) Shi, X.; Zhu, G.; Wang, X.; Li, G.; Fang, Q.; Wu, G.; Tian, G.; Xue, M.; Zhao, X.; Wang, R.; Qiu, S. From a 1-D Chain, 2-D Layered Network to a 3-D Supramolecular Framework Constructed from a Metal-Organic Coordination Compound. *Cryst. Growth Des.* **2005**, *5*, 207−213.
(60) Grabowski, S. J. *Understanding Hydrogen Bonds: Theoretical and Experimental Views*; Royal Society of Chemistry: United Kingdom, 2021.

https://doi.org/10.1021/acsomega.2c00447
ACS Omega 2022, 7, 13067−13074